Effect of Dynamic Creep Coefficients and External Load on Hunting Velocity in a Railway Vehicle

Seyed Ali Mousavi, Kourosh Heidari Shirazi[*]**, Laleh Fatahi**

Mechanical Engineering Department, Faculty of Engineering, Shahid Chamran University of Ahvaz, Ahvaz, Iran
sa-mousavi@stu.scu.ac.ir; k.shirazi@scu.ac.ir; lfatahi@scu.ac.ir

Abstract: The purpose of this research is to provide an accurate and low degree of freedom model to analyze critical hunting velocity for a rail vehicle. Two types of simplifications have been commonly used in investigations, including linearization of nonlinear and trigonometric terms and applying static coefficients in linear wheel/rail contact models such as Kalker model. To find the effect of these simplifications in the accuracy of computed hunting velocity a 3DOF single-axis bogie model with a wheelset possessing 3D motion mobility and constant wheel/rail contact is used. The creep forces and spin moment in the contact model are obtained from the linear Kalker model with dynamic creep coefficients. The contact model coefficients are updated in each moment based on the instant values of normal wheel force and wheelset yaw angle using a proposed algorithm. The critical speed and bifurcation diagram of the hunting frequencies are obtained and a comparison is made between the static creep coefficient model and dynamic creep coefficient model. According to the results, dramatic changes in stability margins and starting point of period doubling in the bifurcation diagram are observed under the presence of dynamic creep coefficients. Also, an increase of normal external load on the wheelset causes the reduction of critical velocity, which is merely predicted in the dynamic coefficient model. This means the static creep coefficient models do not have enough reliability for analyzing the variable weight wagon problems such as freight trains. Another important result is that the simplification of most trigonometric terms has a negligible effect on the accuracy of results.

Keywords: Creep Forces; Creep Coefficients; Stability; Hunting; Bifurcation

1   Introduction

Railway transportation has been played an important role in today's human life. Needs for higher-speed trains to increase the capacity of transportation systems besides the aging of the railway networks arises new engineering and technical challenges for designers. One of the important problems in the field of stability of

the rail vehicles dynamics is hunting behavior. The hunting can lead to an unstable amplitude growth in vibration about the yaw axis of the suspension system (or bogie) that can be ended by wagon derailment. That is why determining the accurate margin of the hunting is of great importance in the multi-body dynamics of rail vehicles. The hunting is inevitable and roots in the intrinsic property of conical wheelset, creep forces, and bogie's mass-stiffness-damper interactions in a parallel rail system. Also, it reduces ride comfort and causes damage to vehicles and rail.

Ahmadian and Yang [1, 2] evaluated the effect of system parameters on the stability of the railway vehicle by considering the nonlinear parameters of yaw damper and wheel-rail contact. The numerical simulation showed that damping coefficient changes could change the critical hunting speed. They also analyzed the Hopf bifurcation phenomenon. The results showed that nonlinear parameters in the primary suspension system, as well as rail and wheel flange contact, will play a significant role in hunting behavior. Also, nonlinear elements in wheel and rail contact and suspension systems affect critical speed and bifurcation. In some cases, the results show that the critical velocity obtained from the linear analysis is higher, than that obtained from the nonlinear analysis. In the work of True and Asmund [3], the dynamic analysis of a freight wagon in the presence of dry friction damper and nonlinear creep forces in the contact area of the wheel and rail was performed. In another work, Lee and Cheng [4, 5], employed Lyapunov's Indirect Method to obtain the critical hunting velocity, under the effects of several physical parameters. They compared the results of their model with a 6 DOF model and observed that the predicted critical hunting speed by the 6 DOF system is much higher than their model. Another interesting finding of this work was that the critical hunting velocity of wagons with new wheels is more than that with worn wheels. Using a nonlinear creep model, Lee and Cheng [6, 7] derived the equations of motion for an 8 DOF system. They compared the results of the 8 DOF model with a 6 DOF model in a curved path. Unlike the previous studies, their investigations showed that the critical hunting velocity for the 8 DOF model is higher than the 6 DOF model, However, they both used nonlinear models, predicting fewer hunting velocities compared with the linear contact model. Also, for 8 DOF model and based on the linear creep model, the effect of the parameters of the secondary suspension system on the critical speed was investigated. Zeng and Wu [8] examined the derailment of a rail vehicle by considering the contact angle of the wheel flange, the coefficient of friction, the creep forces, and the presentation of a new relationship. The results showed that increasing the contact angle of the wheel rim and reducing the coefficient of friction is effective in preventing wheel climb derailment. Cheng et al. [9] used a nonlinear heuristic creep model for a 21 DOF wagon model and obtained the critical speed of the wagon as it crossed the curved track. Their results showed that the critical speed obtained for a 6 and a 14 DOF models is much higher than the 20 DOF model. Also, the critical velocity obtained by the nonlinear heuristic creep model is lower than the velocity obtained from the linear creep model. Zboinski and Dusza [10]

studied the stability and self-excited vibrations of a rail vehicle on a curved track and used the fork diagrams for the curved track to examine the effect of different initial conditions. Kim and Seok [11] used the multiple-scale method to study the bifurcation diagrams of a rail vehicle using linear and nonlinear models for lateral wheelset displacements. By presenting a dynamic model of a rail vehicle, Wang and Li [12, 13] investigated the effect of acceleration on the wheel lift. It was observed that the contact patch of the wheel and rail at a contact angle has a critical point, to start the derailment occurs quickly. Zhang and Dai [14] presented a mathematical model of a 2 DOF for a wheelset, to analyze the effect of a yaw damper of secondary suspension on Hopf bifurcation. They also applied the nonlinear contact model of the wheel and the rail, to extract the equations of motion, and study the effect of different parameters on the lateral stability of a particular type of wheelset. Wei and Yabuno [15] examined subcritical Hopf and saddle-node bifurcations in the hunting motion of a railway vehicle by considering cubic and quintic nonlinearities. The results showed that both the cubic and the quintic nonlinearities of the wheel system play an important role. Skerman et al. [16] have investigated the hunting of an unloaded freight wagon fitted with three-piece bogies, which utilize friction wedges for damping and have friction at many interfaces. Several methods of analysis were compared, including simulation on track with irregularities. Also, different initial conditions were used for each bogie to excite different types of hunting at a given speed.

In the present study, the influence of two types of simplifications that are commonly used in the prediction of the hunting velocity, including linearization of nonlinear and trigonometric terms and employing linear contact models with constant coefficients are investigated. In Section 2 dynamic and kinematic equations of motion based on the 3D mobility of wheelset and constant contact of the wheel/rail are derived. In Section 3 linear Kalker model is represented and an algorithm for estimation of dynamical creepage constants is developed. In Section 4, the results are demonstrated and discussed. In Section 5, concluding remarks are presented. The proposed technique could also be useful for the dynamic analysis of two-wheeled robots [17].

2   Governing Equation of a Wheelset

The governing equations of the system include three types of equations, i.e., dynamic equilibrium equations, kinematic compatibility equations, and creepage model constitutive equations for creepage forces and moments. According to Figure 1, to describe the three-dimensional rotation of the wheelset with respect to the ground frame, three coordinate systems with three associated rotations including, ψ rotation angle about the vertical axis (or Z) and φ rotation angle about the longitudinal axis (or X), and θ angular velocity about wheelset lateral

axis can be used. Therefore, the angular velocity of the wheelset and velocity of wheelset midpoint are obtained as follows:

$$\vec{\omega} = \dot{\varphi}\hat{i}_1 + (\Omega + \dot{\theta})\hat{j}_w + \dot{\psi}\hat{k} \tag{1}$$

$$\vec{v} = (V + \dot{x})\hat{i} + \dot{y}\,\hat{j} + \dot{z}\,\hat{k} \tag{2}$$
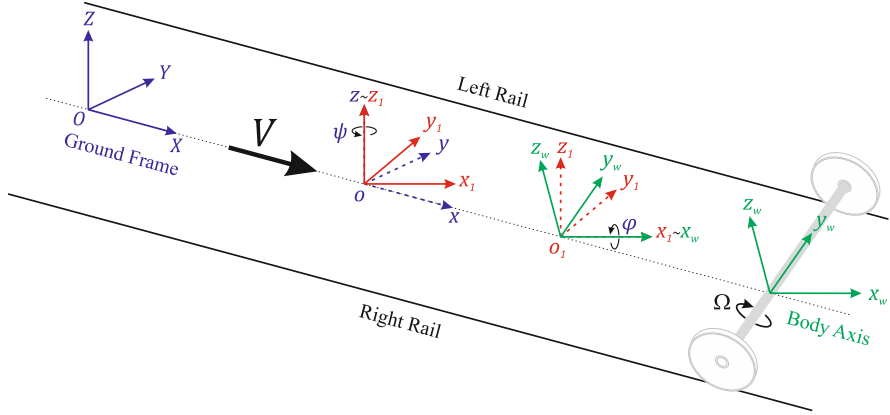
Figure 1

Axes Systems of Wheelset

where, V and Ω are constant parts and $\dot{x}$ and $\dot{\theta}$ are variable parts of the components v_x and ω_y, respectively.

2.1   Kinematics of the Wheelset Contact Point

The front view of the wheelset, normal and tangential components of contact forces, and also the geometry of the wheelset are depicted in Figure 2. By using Figure 2 the position vectors of the contact point for the left and right wheel with respect to the wheelset midpoint are given as follows:
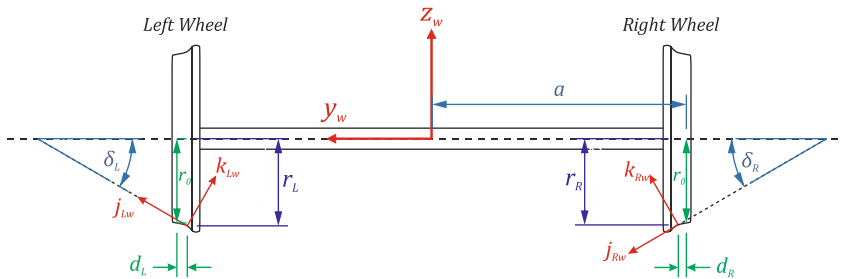
Figure 2

Contact Axes

$$\vec{r}_c^{\,Lw} = (a - d_L)\,\hat{j}_w - r_L \hat{k}_w \tag{3}$$

$$\vec{r}_c^{\,Rw} = -(a + d_R)\,\hat{j}_w - r_R \hat{k}_w \tag{4}$$

where, a is half-track length. Using proper coordinate transformations, the normal forces can be obtained for each wheel:

$$\vec{N}_L^w = \begin{Bmatrix} N_L \sin(\psi)\sin(\delta_L + \varphi) \\ -N_L \cos(\psi)\sin(\delta_L + \varphi) \\ N_L \cos(\delta_L + \varphi) \end{Bmatrix} \begin{matrix} i \\ j \\ k \end{matrix} \tag{5}$$

$$\vec{N}_R^w = \begin{Bmatrix} -N_R \sin(\psi)\sin(\delta_R - \varphi) \\ +N_R \cos(\psi)\sin(\delta_R - \varphi) \\ N_R \cos(\delta_R - \varphi) \end{Bmatrix} \begin{matrix} i \\ j \\ k \end{matrix} \tag{6}$$

Moreover, the angular velocity of the left and right wheel can be expressed in the left and right wheels frames as follows:

$$\vec{\omega}_c^{\,Lw} = \begin{Bmatrix} \dot{\varphi} \\ +(\Omega + \dot{\theta})\cos\delta_L + \dot{\psi}\sin(\delta_L + \varphi) \\ -(\Omega + \dot{\theta})\sin\delta_L + \dot{\psi}\cos(\delta_L + \varphi) \end{Bmatrix} \begin{matrix} i_{Lw} \\ j_{Lw} \\ k_{Lw} \end{matrix} \tag{7}$$

$$\vec{\omega}_c^{\,Rw} = \begin{Bmatrix} \dot{\varphi} \\ +(\Omega + \dot{\theta})\cos\delta_R - \dot{\psi}\sin(\delta_R - \varphi) \\ +(\Omega + \dot{\theta})\sin\delta_R + \dot{\psi}\cos(\delta_R - \varphi) \end{Bmatrix} \begin{matrix} i_{Rw} \\ j_{Rw} \\ k_{Rw} \end{matrix} \tag{8}$$

where, $\vec{r}_c^{\,Lw}$ and $\vec{r}_c^{\,Rw}$ are position vectors of the left and right contact points relative to the center of the wheelset in the corresponding frames, $\vec{N}_L^w$ and $\vec{N}_L^w$ are normal forces in the ground frame.

2.2   Equation of Motion for the Wheelset

Considering dynamic equilibrium and ground frame the equations of motion can be derived using the well-known Newton's second law as follows:

$$m\ddot{\vec{r}} = \Sigma \vec{F} \tag{9}$$

$$\dot{\vec{H}}_G = \Sigma \vec{M}_G \tag{10}$$

Using, Figure 3 and substituting the wheelset's mass, inertia, midpoint acceleration, and angular velocity and exerting external forces and moments in Eqs. 9 and 10, six Eqs. 11 to 16 will be obtained for the model of a wheelset shown in Figure 3:
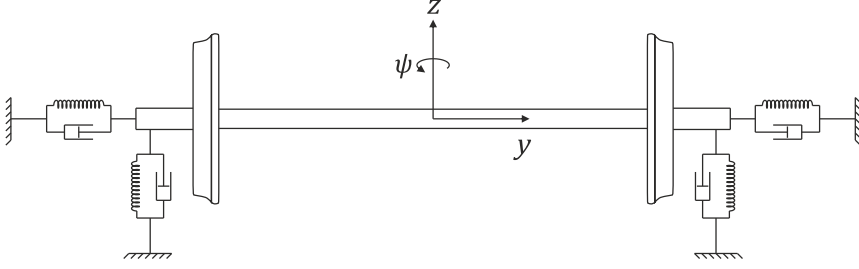
Figure 3
Model of Wheelset

$$m_w \ddot{x} = F_{lx} + F_{rx} + N_{lx} + N_{rx} \tag{11}$$

$$m_w \ddot{y} = F_{ly} + F_{ry} + N_{ly} + N_{ry} + F_s - F_T \tag{12}$$

$$m_w \ddot{z} = F_{lz} + F_{rz} + N_{lz} + N_{rz} - m_w g - W_{ext} \tag{13}$$

$$I_x \ddot{\varphi} \cos \psi + u \left(\varphi \mathbf{f} \dot{\varphi}, \dot{\theta}, \ddot{\theta}, \psi, \dot{\psi}, \ddot{\psi} \right) = + R_{ry} \left(F_{rz} + N_{rz} \right)$$
$$- R_{rz} \left(F_{ry} + N_{ry} \right) + R_{ly} \left(F_{lz} + N_{lz} \right) - R_{lz} \left(F_{ly} + N_{ly} \right) + M_{lx} + M_{rx} + M_{sx} \tag{14}$$

$$I_y \ddot{\theta} \cos \varphi \cos \psi + v \left(\varphi, \dot{\varphi}, \ddot{\varphi}, \dot{\theta}, \psi, \dot{\psi}, \ddot{\psi} \right) = + R_{rx} \left(F_{rz} + N_{rz} \right)$$
$$- R_{rz} \left(F_{rx} + N_{rx} \right) + R_{lx} \left(F_{lz} + N_{lz} \right) - R_{lz} \left(F_{lx} + N_{lx} \right) + M_{ly} + M_{ry} + M_{sy} \tag{15}$$

$$\left(I_z \cos^2 \varphi + I_y \sin^2 \varphi \right) \ddot{\psi} + w \left(\varphi, \dot{\varphi}, \dot{\theta}, \ddot{\theta}, \dot{\psi} \right) = + R_{rx} \left(F_{ry} + N_{ry} \right)$$
$$- R_{ry} F_{rx} + R_{lx} \left(F_{ly} + N_{ly} \right) - R_{ly} F_{lx} + M_{lz} + M_{rz} + M_{sz} - 2b F_d \tag{16}$$

where, F_{ij}, M_{ij} and N_{ij} are creep forces, moments, and normal forces, respectively and R_{ij} are moment arms and $i = \{l, r\}$ & $j = \{x, y, z\}$. Also, suspension force F_s, suspension moment M_s, flange force F_T, and yaw damper moment $2b F_d$ can be derived as follows [2]:

$$\vec{F}_s = -2 \left(K_y y + C_y \dot{y} \right) \hat{j} \tag{17}$$

$$\vec{M}_s = -2 K_\psi b^2 \psi \tag{18}$$

$$F_T = \begin{cases} K_r \left(y - \delta \right) & y > \delta \\ 0 & -\delta < y < \delta \\ -K_r \left(y + \delta \right) & y < -\delta \end{cases} \tag{19}$$

$$F_d = \begin{cases} C_1 V_\psi + C_2 V_\psi^2 + C_3 V_\psi^3 + C_4 V_\psi^4 & V_\psi > 0 \\ C_1 V_\psi - C_2 V_\psi^2 + C_3 V_\psi^3 - C_4 V_\psi^4 & V_\psi < 0 \end{cases} \tag{20}$$

Eqs. 12 and 16 will be used as the main equations to derive lateral displacement y and the yaw angle ψ. Two unknowns $\dot{x}$ and $\dot{\theta}$ in Eqs. 11 and 15, and the vertical forces of the left and right wheels in Eqs. 13 and 14 can be derived using the two following kinematic constraints:

$$z = -\frac{\lambda a\left(1-cos\psi\right)}{cos\psi} + \frac{\lambda a y^2}{\left(a-\lambda r_0\right)^2} \tag{21}$$

$$\varphi = \frac{\lambda y}{a-\lambda r_0} \tag{22}$$

2.3 The Creep Forces and Moments

Large forces are generated in the contact area of wheels and rails, and these forces have a significant effect on the dynamics of the vehicle. Among the various modeling methods for approximating the creep forces and moments in the wheel-rail contact patch, Kalker theory [18] is extensively used in the applications. According to Kalker theory, if the longitudinal, lateral, and spin creep parameters are very small, the slip zone is small, and therefore, regardless of slip, the adhesion zone can be considered as the dominant area in wheel-rail contact. Based on this theory, creep forces and spin moment are defined through Eqs. 23, 24, and 25:

$$F_x = -f_{33}\xi_x \tag{23}$$

$$F_y = -f_{11}\xi_y - f_{12}\xi_{sp} \tag{24}$$

$$M_z = f_{12}\xi_y - f_{22}\xi_{sp} \tag{25}$$

where, f_{11}, f_{12}, f_{22}, and f_{33} are the creep coefficients and ξ_x, ξ_y and ξ_{sp} are creepage terms. Since the creep forces are defined on the wheel contact plane they should be expressed with respect to the ground frame.

2.4 Creepage Expressions

When two relatively rigid bodies are compressed and rolled, a creep phenomenon occurs, and creep forces are generated. These forces have a significant effect on the dynamic behavior of the wheel and eventually railway vehicles. Based on Carter's work [19] the left and right wheel creepage can be computed as follows:

$$\xi_x^L = \frac{1}{V}\Big[+\left(V+\dot{x}\right)\cos\psi + \dot{y}\sin\psi - r_L\dot{\psi}\sin\varphi - \left(a-d_L\right)\dot{\psi}\cos\varphi - \left(\Omega+\dot{\theta}\right)r_L\Big] \tag{26}$$

$$\xi_y^L = \frac{1}{V}\Big[-(V+\dot{x})\cos(\delta_L+\varphi)\sin\psi + \dot{y}\cos(\delta_L+\varphi)\cos\psi$$
$$+\dot{z}\sin(\delta_L+\varphi)+r_L\dot{\varphi}\cos\delta_L+(a-d_L)\dot{\varphi}\sin\delta_L\Big] \tag{27}$$

$$\xi_{sp}^L = \frac{1}{V}\Big[-(\Omega+\dot{\theta})\sin\delta_L+\dot{\psi}\cos(\delta_L+\varphi)\Big] \tag{28}$$

$$\xi_x^R = \frac{1}{V}\Big[+(V+\dot{x})\cos\psi + \dot{y}\sin\psi - r_R\dot{\psi}\sin\varphi+(a+d_R)\dot{\psi}\cos\varphi-(\Omega+\dot{\theta})r_R\Big] \tag{29}$$

$$\xi_y^R = \frac{1}{V}\Big[-(V+\dot{x})\cos(\delta_R-\varphi)\sin\psi + \dot{y}\cos(\delta_R-\varphi)\cos\psi$$
$$-\dot{z}\sin(\delta_R-\varphi)+r_R\dot{\varphi}\cos\delta_R+(a+d_R)\dot{\varphi}\sin\delta_R\Big] \tag{30}$$

$$\xi_{sp}^R = \frac{1}{V}\Big[(\Omega+\dot{\theta})\sin\delta_R+\dot{\psi}\cos(\delta_R-\varphi)\Big] \tag{31}$$

2.5   Creep and Creepage Coefficients

The creep coefficient f_{11}, f_{12}, f_{22}, and f_{33} are defined as follows:

$$f_{11} = (ab)GC_{22} \tag{32}$$

$$f_{12} = (ab)^{3/2}GC_{23} \tag{33}$$

$$f_{22} = (ab)^2GC_{33} \tag{34}$$

$$f_{33} = (ab)GC_{11} \tag{35}$$

where, C_{11}, C_{22}, C_{23}, and C_{33} are the creepage and spin coefficients, which depend only on Poisson's ratio (υ) and the ratio of the semi-axis of the contact ellipse (a/b) according to Kalker table of creepage and spin coefficients. Given G and υ, combined rigidity modulus, and combined Poisson's ratio, respectively, as follows:

$$G = \frac{2G_wG_r}{G_w+G_r} \tag{36}$$

$$\upsilon = \frac{G}{2}\left[\left(\frac{\upsilon_w}{G_r}\right)+\left(\frac{\upsilon_w}{G_r}\right)\right] \tag{37}$$

where, a and b are the semi-axis of the contact ellipse in the rolling direction and lateral direction, respectively, such that [20]:

$$a = m\left[3\pi N\left(K_1 + K_2\right)/4K_3\right]^{1/3} \tag{38}$$

$$b = n\left[3\pi N\left(K_1 + K_2\right)/4K_3\right]^{1/3} \tag{39}$$

where, N is the normal force, and subscripts w and r denote wheel and rail, respectively and K_1, K_2 and K_3 are defined as follows:

$$K_1 = \frac{1 - \upsilon_w^2}{\pi E_w} \tag{40}$$

$$K_2 = \frac{1 - \upsilon_r^2}{\pi E_r} \tag{41}$$

$$K_3 = \frac{1}{2}\left[\frac{1}{R_w} + \frac{1}{R'_w} + \frac{1}{R_r} + \frac{1}{R'_r}\right] \tag{42}$$

where, R, R' and E denote the rolling radius of the wheel, the transverse radius of curvature of the wheel profile at the point of contact, and Young's modulus of elasticity, respectively.

Given θ and K_4/K_3, the coefficients m and n in Eqs. 38 and 39 can be estimated using Table of Hertz [20], where θ and K_4 are defined as follows:

$$\theta = cos^{-1}\left(K_4/K_3\right) \tag{43}$$

$$K_4 = \frac{1}{2}\left[\left(\frac{1}{R_w} + \frac{1}{R'_w}\right)^2 + \left(\frac{1}{R_r} + \frac{1}{R'_r}\right)^2 + 2\left(\frac{1}{R_w} - \frac{1}{R'_w}\right)\left(\frac{1}{R_r} + \frac{1}{R'_r}\right)\cos\left(2\psi\right)\right] \tag{44}$$

where, ψ is the angle between the normal planes that contain the curvatures $1/R_1$ and $1/R_2$ such that when the rails are parallel, ψ is the yaw angle of the wheel about the vertical axis.

According to the above-mentioned equations, an algorithm can be suggested for the dynamic updating of creep coefficients. The process of estimation of creep forces includes manipulation of, creepage expressions computation, creepage coefficients, and creep coefficients. The former is obtained from kinematic variables and the latter from the wheel normal force and yaw angle. The flowchart in Figure 4 represents this dependency and order of calculations of the variables. In this flowchart, the yellow boxes contain the constant parameters depending on the mechanical properties of the wheels and rails, the white boxes contain parameters that are a function of the normal wheel force and the yaw angle, and gray boxes contain input variables of the normal wheel force and the yaw angle.

All these boxes stepwise contribute to computing the instant values of creep forces. It should be noted that finding some of the parameters such as creepage coefficients ($\equiv C_{ij}$), m and n requires linear interpolation/extrapolation between the tabular data, which is a source of inaccuracy, especially when due to the dynamic interaction of the wheel/rail, the instant values of K_4, a and b are not constant. One way of eliminating these inaccuracies is to replace the tables with curve-fitting nonlinear functions.

Figure 4

Creep forces flowchart

2.6 Curve Fitting of Creep Coefficients

One of the tables that should be replaced by curve fitting functions is the table of creepage and spin coefficients (including four tables each for one of the coefficients C_{ij}'s; C_{11}, C_{22}, C_{33} and C_{23}). In each table, ten columns are containing ten values of the ratio of the elliptical diameters of the contact patch and three rows contain values of Poisson's ratio 0, 0.25, and 0.5, which forms a total of 30 data points. As a beneficial tool for the selection and parameter estimation of the interpolation functions, Matlab-CFtool is utilized. Using this tool the user would be able to examine various predefined functions for fitting the data with the least R-square (R^2). In the first step, in each table using the quadratic polynomials, values of four C_{ij}'s, for $v = 0.28$, are estimated. A three-parameter

power function for curve fitting is employed to fit ten values of elliptical diameter ratios for row $v = 0.28$:

$$C_{ij} = c_1 \left(\frac{b}{a} \right)^{c_2} + c_3 \tag{45}$$

where, c_1, c_2 and c_3 are three function parameters. Table 1 summarizes the three parameters of each of the power functions for each of C_{ij}'s table. These functions are depicted in Figure 5 (a) to (d). To ensure the accuracy of estimation of each function the value of R-square is represented in Table 1.

Table 1
Power function curve fitting of creepage and spin coefficients for $v = 0.28$

Coefficient	c_1	c_2	c_3	R^2
C_{11}	1.2460	-0.8524	2.9650	1
C_{22}	1.6650	-0.8238	2.0310	1
C_{23}	0.8630	-1.2200	0.6391	1
C_{33}	0.7695	+1.0080	0.4180	0.9999

For estimation of m and n using the Hertz table [20], two types of function are employed, including a three-parameter power function m and a four-parameter exponential function n. These functions are selected using the evaluation of the R-square of the CFtool different functions. Based on the calculations, the functions are as follows: $m = 37.44\theta^{-0.7236} - 0.451$ $\left(R^2 = 1 \right)$ (46)

$$n = 0.3626 \exp(0.0113\theta) - 0.259 \exp(-0.107\theta) \qquad \left(R^2 = 0.9995 \right) \tag{47}$$

The curve of the functions of m and n are depicted in Figure 5 (e) and (f).

(a) C_{11} (b) C_{22}

(c) C_{23}

(d) C_{33}

(e) $m - \theta$

(f) $n - \theta$
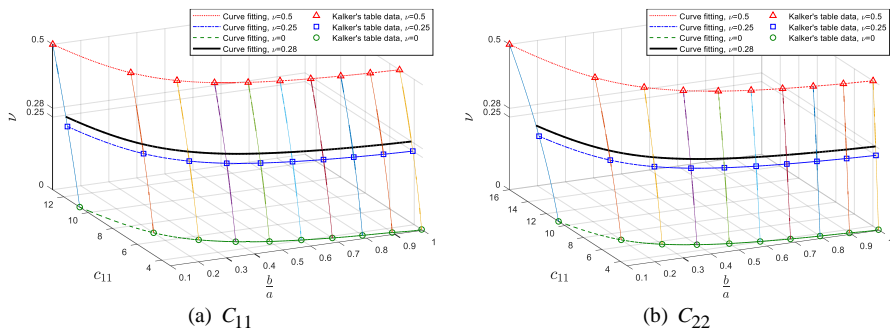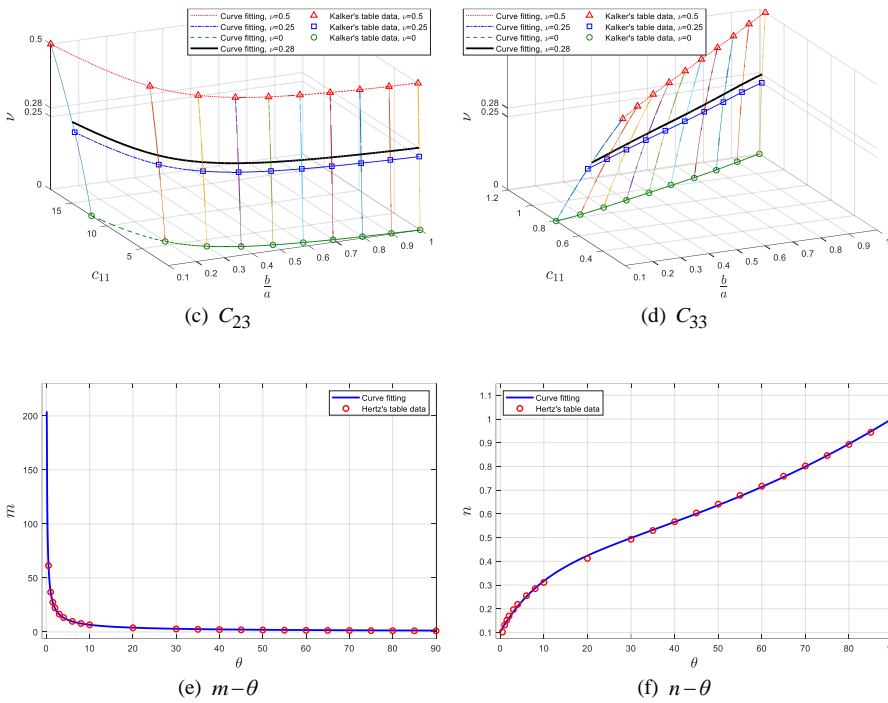
Figure 5
Creep Coefficients Curve Fitting

3 Results

In this section, several studies are performed to clear both the effect of simplification by comparing a simplified 2DOF, with a full terms 3DOF model, as well as the effect of contact model by comparing a static creep coefficient (SCC) model and a dynamic creep coefficient (DCC) model. The numerical values of the parameters and constants of the system are summarized in Table 2. The first study results are depicted in Figure 6. In this study, nonlinear and trigonometric terms of the mathematical model of the considered system are neglected, however, two systems are considered, which are, the simplified model with SCC as well as the simplified model with DCC. Also for the purpose of validation, the results are compared with those presented in [21]. The results are included a bifurcation diagram of lateral vibration amplitude of the wheelset under the velocity up to $60\,m/s$ and for three cases of vertical external loading, exerted on the midpoint of the wheelset. It is seen that the results of SCC model are very similar to that of [21] and the increase of external load has no significant effect on the hunting velocity, by which, jumping on the lateral vibration amplitude occurs.

However, for DCC surprisingly a dramatic reduction of hunting velocity for higher external loads is observed. Practically, this means that the heavier the wagon, the more instability and lower the critical velocity.
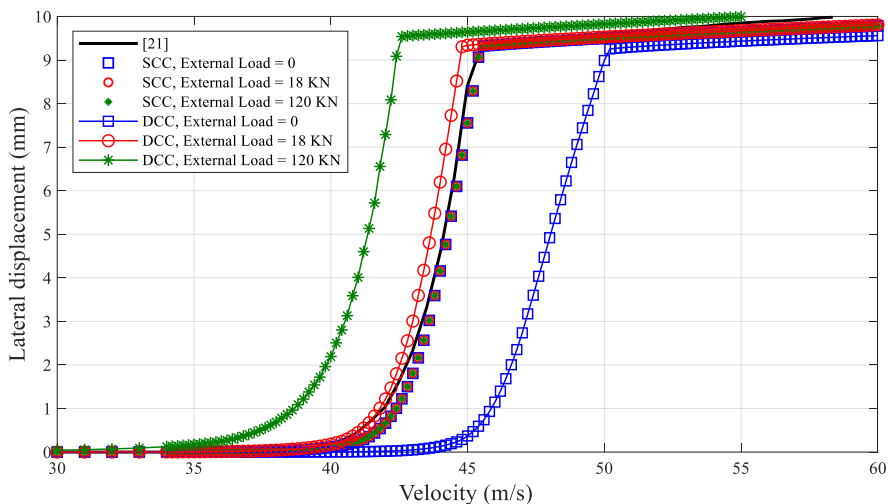
Figure 6

Comparison of bifurcation diagrams for lateral displacement from the simplified equations of motion with Reference [21]

Table 2

System Parameters [2]

Half of the track gauge	$a = 0.7176\,m$
Half of yaw spring arm	$b = 1\,m$
Lateral damping of suspension	$C_y = 2.1 \times 10^4\ N.s\,/\,m$
Damping coefficients for yaw dampers	$C_1 = 1.9230 \times 10^4$
	$C_2 = 5.1400 \times 10^5$
	$C_3 = 3.1127 \times 10^6$
	$C_4 = 5.1400 \times 10^6$
Lateral creep force coefficient	$f_{11} = 6.728 \times 10^6\ N$
Spin creep force coefficient	$f_{22} = 1000\ N.m^2$
Lateral spin creep force coefficient	$f_{12} = 1.2 \times 10^3\ N.m$
Longitudinal creep force coefficient	$f_{33} = 6.728 \times 10^6\ N$
Roll moment of inertia of wheelset	$I_{wx} = 625.7 kg.m^2$

Spin moment of inertia of wheelset	$I_{wy} = 133.92\,kg.m^2$
Lateral rail stiffness	$K_r = 1.617 \times 10^7\,N/m$
Lateral stiffness of primary suspension	$K_y = 8.67 \times 10^4\,N/m$
Yaw spring stiffness of primary suspension	$K_x = 8.67 \times 10^4\,N/m$
Wheelset mass	$m_w = 1800\,kg$
Wheel radius	$r_0 = 0.533\,m$
Wheel conicity	$\lambda = 0.05$
Flange clearance	$\delta = 0.923\,cm$

The second study focuses on the effect of degrees of freedom of the model and the effect of the presence of nonlinear terms and additional degrees of freedom in the model. The considered model is a 3DOF model, with 6 generalized coordinates including, x , y , z , φ , ψ and θ . However, because of the presence of the three geometrical constraints, the remaining DOF is 3, e.g., y , ψ and x . Meanwhile, there is a simplified 2DOF model, which is extensively used in nonlinear and perturbation analyses [1], which merely considers y and ψ 2DOF. According to this model, $\dot{x}$ and $\dot{\theta}$ are assumed to be constant. The diagrams in Figure 7 to Figure 9, show that the 2 DOF and 3DOF models have similar responses under the different vertical external loading conditions, whether the model is of SCC type or DCC.

(a) Static Creep Coefficients   (b) Dynamic Creep Coefficients
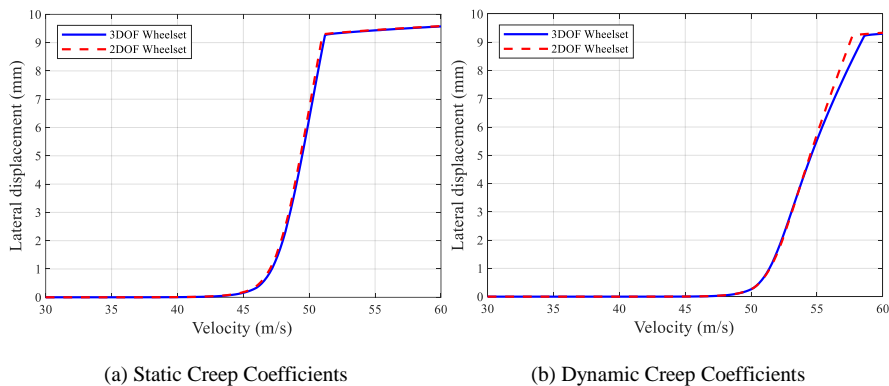
Figure 7
Comparison of 2DOF and 3DOF results, Axle Load $= 0$

(a) Static Creep Coefficients   (b) Dynamic Creep Coefficients
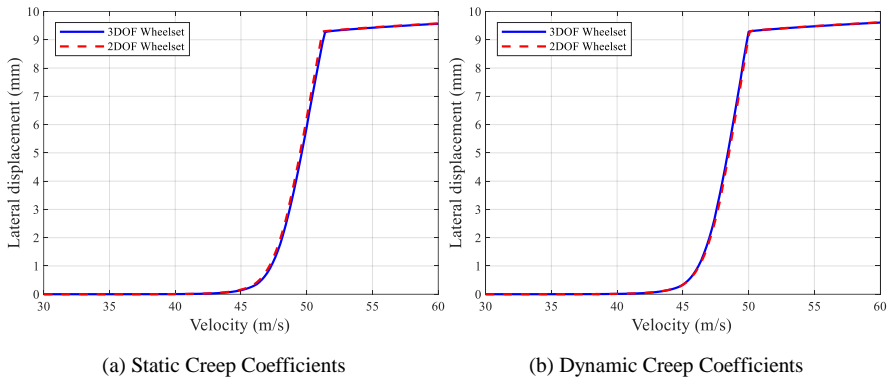
Figure 8
Comparison of 2DOF and 3DOF results, Axle Load $= 18\,KN$

(a) Static Creep Coefficients   (b) Dynamic Creep Coefficients
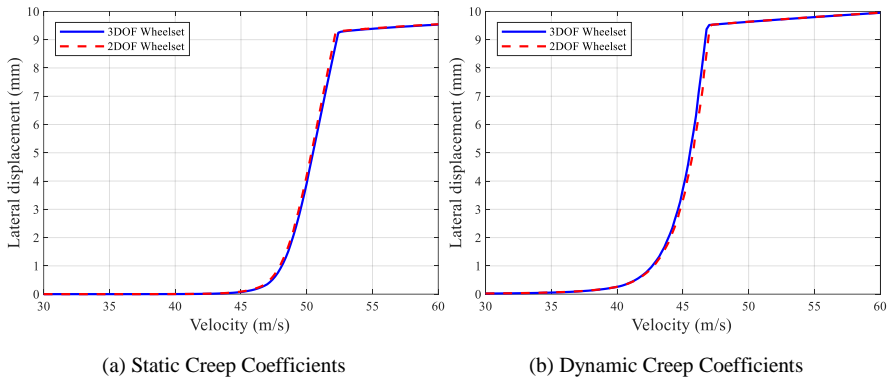
Figure 9
Comparison of 2DOF and 3DOF results, Axle Load $= 120\,KN$

(a) Time Response   (b) Frequency Response
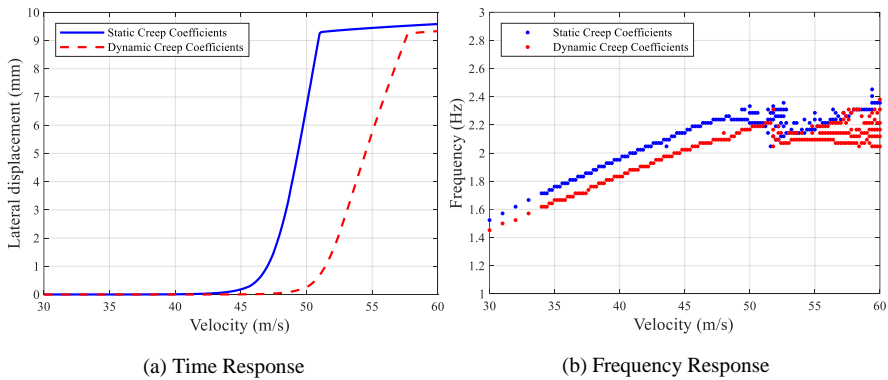
Figure 10
Comparison of bifurcation diagrams for lateral displacement, Axle Load $= 0$

(a) Time Response   (b) Frequency Response
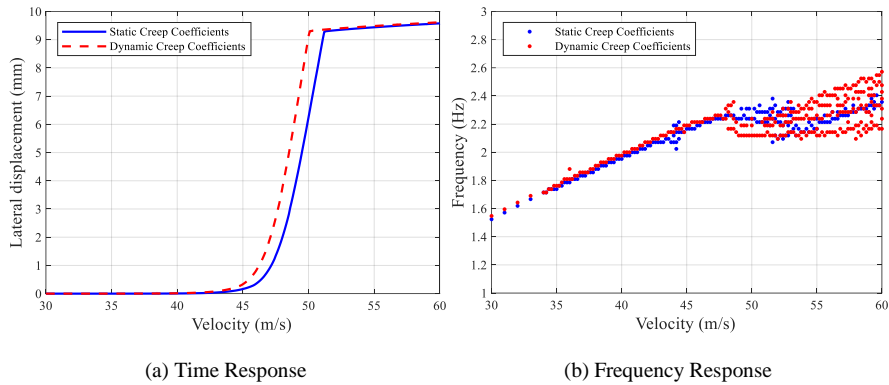
Figure 11
Comparison of bifurcation diagrams for lateral displacement, Axle Load $=18\,KN$

(a) Time Response   (b) Frequency Response
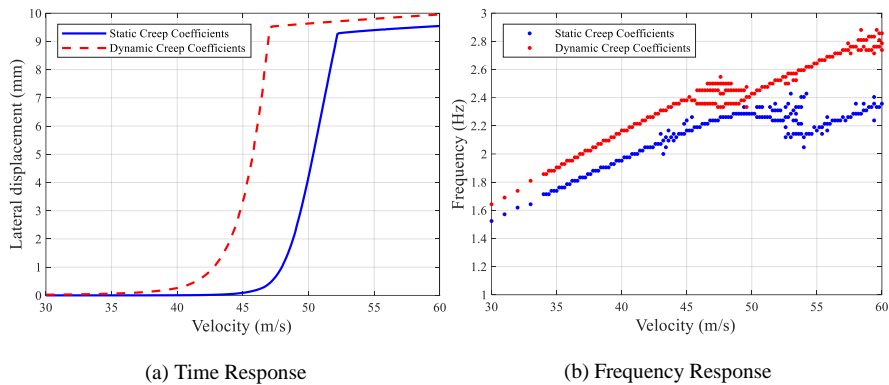
Figure 12
Comparison of bifurcation diagrams for lateral displacement, Axle Load $=120\,KN$

In the third study, the importance of creep coefficients on the regularity of lateral dynamic behavior of the wheelset is investigated. To this end, the lateral response amplitude of the two SCC 3DOF and DCC 3DOF models under the different vertical loads are analyzed. In addition to the amplitude, the frequency content of the time domain response of the lateral vibration in the different forward velocities are extracted. According to Figure 10(a) to Figure 12(a) not only the DCC model predicts that increase of the vertical external load, causes a decrease in the hunting velocity, but also from Figure 10 (b) to Figure 12(b) it is concluded that the DCC model predicts that entering the behavior to a period-doubling process and burst the chaotic dynamic is more probable for the smaller vertical external loads.

The latter means that as it is depicted from Figure 12(b) the regularity in lateral dynamic behavior for a vertical external load $120\,KN$ is much more than $18\,KN$ and

$0\,KN$ cases. While the bifurcation diagram drawn by SCC model has no significant difference for the different vertical external loads.

Another example of the remarkable effect of DCC in the prediction of hunting at different speeds is shown in Figure 13. According to Figure 13 in $55\,m/s$ both the SCC and DCC models predict unstable vibration such that rail-flange contact occurs. However, for the unload case in Figure (a) and Figure (d), the DCC model reports the presence of a stable limit cycle while the SCC model reports unstable growth of amplitude which ends with the flange contact. Also, according to Figure 13(c) and Figure 13(e) and imminent derailment is predicted by the DCC model while the SCC model shows more safe motion. Figure 13 clearly proofs that predictions and interpretations of the DCC model in many cases completely differ from those of the SCC model.

| (a) SCC, Axle Load $= 0$ | (b) SCC, Axle Load $= 18\,KN$ | (c) SCC, Axle Load $= 120\,KN$ |
| (d) DCC, Axle Load $= 0$ | (e) DCC, Axle Load $= 18\,KN$ | (e) DCC, Axle Load $= 120\,KN$ |
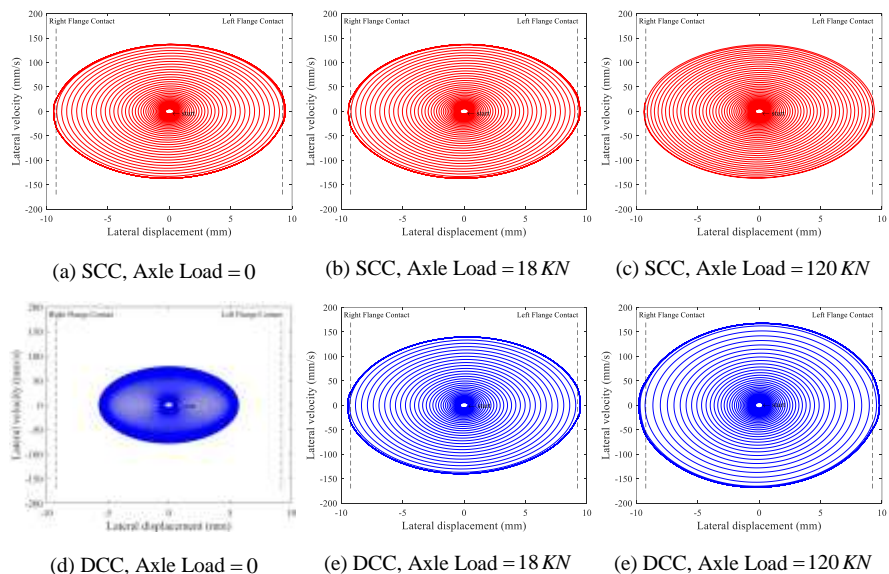
Figure 13

Phase portrait plot for the 3DOF wheelset in velocity $55\frac{m}{s}$

Conclusions

In the present work, the effect of some factors in the final prediction of the hunting velocity of a railway vehicle such as the mathematical contact model, degree of freedom of the wheelset, dynamic creep coefficients, and the presence of small nonlinearities in the model have been studied. A simplified 2DOF model and a 3DOF full terms dynamic models are considered. Also, two contact models based on the linear Kalker model with the assumption of SCC and DCC have been compared. The phase diagram as well as amplitude and frequency bifurcation

diagrams for different ranges of velocity and external vertical loads have been generated. The results can be summarized as follows:

The presence of all trigonometric and small nonlinearities in the 3DOF model has no particular effect on the accuracy of results compared to the simplified 2DOF model.

Bogie models with SCC contact assumption are not able to predict the dependency of the hunting velocity to the vertical external load, whereas DCC model show this dependency clearly.

According to the DCC models increase of the external vertical load, causes an increase in the instability of velocity margin and decreases the irregularity during hunting motion.

Due to the important role of external load in hunting velocity, different permissible velocities should be used for the full and empty state of freight trains for more derailment safety.

References

[1]   Ahmadian, M., Yang, S.: Effect of system nonlinearities on locomotive bogie hunting stability. *Veh. Syst. Dyn.*, **29** (6), 1998, pp. 365-384

[2]   Ahmadian, M., Yang, S.: Hopf Bifurcation and Hunting Behavior in a Rail Wheelset with Flange Contact. *Nonlinear Dyn.*, **15** (1), 1998, pp. 15-30

[3]   True, H., Asmund, R.: The Dynamics of a Railway Freight Wagon Wheelset With Dry Friction Damping. *Veh. Syst. Dyn.*, **38** (2), 2002, pp. 149-163

[4]   Lee, S. Y., Cheng, Y. C.: Hunting stability analysis of high-speed railway vehicle trucks on tangent tracks. *J. Sound Vib.*, **282** (3–5), 2005, pp. 881-898

[5]   Lee, S.-Y., Cheng, Y.-C.: Nonlinear Analysis on Hunting Stability for High-Speed Railway Vehicle Trucks on Curved Tracks. *J. Vib. Acoust.*, **127** (4), 2005, pp. 324-332

[6]   Lee, S. Y., Cheng, Y. C.: Influences of the vertical and the roll motions of frames on the hunting stability of trucks moving on curved tracks. *J. Sound Vib.*, **294** (3), 2006, pp. 441-453

[7]   Lee, S.-Y., Cheng, Y.-C.: A New Dynamic Model of High-Speed Railway Vehicle Moving on Curved Tracks. *J. Vib. Acoust.*, **130** (1), 2008, p. 011009

[8]   Zeng, J., Wu, P.: Study on the wheel/rail interaction and derailment safety. *Wear*, **265** (9), 2008, pp. 1452-1459

[9]   Cheng, Y.-C. et al.: Modeling and nonlinear hunting stability analysis of

high-speed railway vehicle moving on curved tracks. *J. Sound Vib.*, **324** (1), 2009, pp. 139-160

[10]   Zboinski, K., Dusza, M.: Self-exciting vibrations and Hopf's bifurcation in non-linear stability analysis of rail vehicles in a curved track. *Eur. J. Mech. A/Solids*, **29** (2), 2010, pp. 190-203

[11]   Kim, P., Seok, J.: Bifurcation analysis on the hunting behavior of a dual-bogie railway vehicle using the method of multiple scales. *J. Sound Vib.*, **329** (19), 2010, pp. 4017-4039

[12]   Wang, W., Li, G.: Development of high-speed railway vehicle derailment simulation – Part I: A new wheel/rail contact method using the vehicle/rail coupled model. *Eng. Fail. Anal.*, **24**, 2012, pp. 77-92

[13]   Wang, W., Li, G.: Development of high-speed railway vehicle derailment simulation – Part II: Exploring the derailment mechanism. *Eng. Fail. Anal.*, **24**, 2012, pp. 93-111

[14]   Zhang, T., Dai, H.: Bifurcation analysis of high-speed railway wheel-set. *Nonlinear Dyn.*, **83** (3), 2016, pp. 1511-1528

[15]   Wei, W., Yabuno, H.: Subcritical Hopf and saddle-node bifurcations in hunting motion caused by cubic and quintic nonlinearities: experimental identification of nonlinearities in a roller rig. *Nonlinear Dyn.*, **98** (1), 2019, pp. 657-670

[16]   Skerman, D. et al.: Determining the critical speed for hunting of three-piece freight bogies: practice versus simulation approaches. *Veh. Syst. Dyn.*, **0** (0), 2021, pp. 1-22

[17]   Wiech, J. et al.: Virtual spring damper method for nonholonomic robotic swarm self-organization and leader following. *Contin. Mech. Thermodyn.*, **30** (5), 2018, pp. 1091-1102

[18]   Kalker, J. J.: Survey of Wheel/Rail Rolling Contact Theory. *Veh. Syst. Dyn.*, **8** (4), 1979, pp. 317-358

[19]   Carter, F. W.: On the Action of a Locomotive Driving Wheel. *Proc. R. Soc. A Math. Phys. Eng. Sci.*, **112** (760), 1926, pp. 151-157

[20]   Garg, V. K., Dukkipati, R. V.: *Dynamics of Railway Vehicle Systems*. 1984

[21]   Sedighi, H. M., Shirazi, K. H.: Bifurcation analysis in hunting dynamical behavior in a railway bogie: Using novel exact equivalent functions for discontinuous nonlinearities. *Sci. Iran.*, **19** (6), 2012, pp. 1493-1501